Pis'ma v ZhETF, vol. 102, iss. 11, pp. 870 – 875

Anisotropic characteristics of the Kraichnan direct cascade in two-dimensional hydrodynamic turbulence

E. A. Kuznetsov[+*×1)], *E. V. Sereshchenko*[+°▽]

[+]*Novosibirsk State University, 630090 Novosibirsk, Russia*

[*]*Lebedev Physical Institute of the RAS, 119991 Moscow, Russia*

[×]*Landau Institute for Theoretical Physics of the RAS, 119334 Moscow, Russia*

[°]*Khristianovich Institute of Theoretical and Applied Mechanics SB RAS, 630090 Novosibirsk, Russia*

[▽]*Far-Eastern Federal University, 690091 Vladivostok, Russia*

Submitted 14 October 2015
Resubmitted 26 October 2015

Statistical characteristics of the Kraichnan direct cascade for two-dimensional hydrodynamic turbulence are numerically studied (with spatial resolution 8192×8192) in the presence of pumping and viscous-like damping. It is shown that quasi-shocks of vorticity and their Fourier partnerships in the form of jets introduce an essential influence in turbulence leading to strong angular dependencies for correlation functions. The energy distribution as a function of modulus k for each angle in the inertial interval has the Kraichnan behavior, $\sim k^{-4}$, and simultaneously a strong dependence on angles. However, angle average provides with a high accuracy the Kraichnan turbulence spectrum $E_k = C_{\rm K}\eta^{2/3}k^{-3}$, where η is enstrophy flux and the Kraichnan constant $C_{\rm K} \simeq 1.3$, in correspondence with the previous simulations. Familiar situation takes place for third-order velocity structure function S_3^L which, as for the isotropic turbulence, gives the same scaling with respect to separation length R and η, $S_3^L = C_3\eta R^3$, but the mean over angles and time $\bar{C}_3$ differs from its isotropic value.

DOI: 10.7868/S0370274X15230125

1. Introduction. Developed two-dimensional hydrodynamic turbulence, in contrast to three-dimensional turbulence, in the inertial interval of scales possesses an additional integral of motion – enstrophy that is a half integral of the squared vorticity $(1/2)\int_s \Omega^2 d\mathbf{r}$. As was demonstrated in 1967 by Kraichnan [1], the existence of this integral generates in the inertial range its own Kolmogorov-type spectrum of turbulence,

$$E(k) \sim k^{-3} \qquad (1)$$

(now called the Kraichnan spectrum). This spectrum corresponds to a constant enstrophy flux toward the small-scale region. Simultaneously, according to [1], a conventional Kolmogorov spectrum $E(k) \sim k^{-5/3}$ is formed at large scales with a constant energy flux directed toward the region of small values of k (inverse cascade). Since the Kraichnan paper in 1967 there were performed many numerical experiments (see [2–9]; a more complete list in [10]) testified in favor of existence of the Kraichnan spectrum. Already in the first numerical experiments (see, e.g., [2]) there was observed the emergence of sharp vorticity gradients (consistent with the high Reynolds number). It corresponds to the formation of the vorticity jumps similar to shock waves with thickness small compared with their length. Based on these observations, Saffman [11] proposed another spectrum, $E(k) \sim k^{-4}$. The Saffman spectrum was obtained under the assumption that the main contribution to the spectrum comes from isotropically distributed vorticity shocks. (It should be noted that in two-dimensional turbulence, the formation of singular vorticity gradients in finite time is forbidden, in accordance with the rigorous theorems [12]; therefore we will call such structures as quasi-shocks.) On the other hand, it follows from simple considerations that the spectrum with such shocks is expected rather to have the Kraichnan type behavior than that predicted by Saffman. The Fourier amplitude Ω_k from one shock will be $\propto k^{-1}$, that immediately yields the spectrum $E(k) \sim k^{-3}$. However, the situation is not too simple. If one assumes that the characteristic length of the step $L \gg k^{-1}$, then the energy distribution from one such step in the k-space has the form of a jet with an apex angle of the order of

[1)]e-mail: kuznetso@itp.ac.ru

$(kL)^{-1}$. For freely decay turbulence as was shown numerically in [10, 13, 14] the spectrum (1) arises owing to vorticity quasi-shocks, which form a system of jets with weak and strong overlapping in the k-space. In their turn, a reason of appearance of quasi-shocks can be regarded due to the compressible features of the so-called di-vorticity, $\mathbf{B} = \nabla \times \Omega \widehat{z}$. For inertial scales this vector field is frozen-in-fluid and its value, in the general case, according to [10, 13–15] can be changed due to the velocity component $\mathbf{v}_n$, normal to the $\mathbf{B}$-line, for which $\operatorname{div} \mathbf{v}_n \neq 0$. This is the origin of compressibility for continuously distributed di-vorticity lines and thereby appearance of quasi-shocks in 2D. Besides, for freely decay turbulence numerically it was established that: (i) in each of such jets, the fall in $E(k)$ at large k is proportional to k^{-3}, which after the angle averaging yields the spectrum (1); (ii) the third-order velocity structure function $S_3^L(\mathbf{R}) = \langle \delta v_\parallel^3 \rangle$ depends proportionally to R^3 (where $\mathbf{R} = \mathbf{r} - \mathbf{r}'$, $\delta v_\parallel$ – the projection of the velocity difference onto the vector $\mathbf{R}$), in complete agreement with the Kraichnan theory.

The main aim of this paper is to study numerically in which extent all the above statistical properties observed in freely decay two-dimensional turbulence remain for the direct (Kraichnan) cascade when the presence of both pumping and viscous damping. Here, we use the same numerical scheme reported in our previous paper [14] with 8192×8192 grid points and periodical boundary conditions. In order to eliminate an influence of the inverse cascade we introduce at very large scales (comparable with the box size) a big damping that allows us to increase the inertial interval for the direct cascade. In the inertial range we put the damping rate equal to zero and switch on the viscous-like dissipation starting from $k = 0.6 k_{\max}$.

The main results of this paper are as follows.

1. The energy spectrum averaged over angles, as a function of modulars k, with a high accuracy has the Kraichnan behavior: $E(k) = C_{\mathrm{K}} \eta^{2/3} k^{-3}$, where η is the enstrophy flux and C_{K} – the Kraichnan constant. In our simulations $C_{\mathrm{K}} \simeq 1.3$, in correspondence with the previous simulations [16–19].

2. The formation of k^{-3}-dependence happens for all rays in the k-space starting from sufficiently earlier evolution times (about two-three characteristic inverse maximal vorticity $\omega_{\max}^{-1}$). However, the angular dependence of energy distribution $\epsilon(\mathbf{k})$, in all our numerical experiments, remains far from isotropic. In k_x–k_y plane it has a very pronounced jet behavior, typical for freely decay turbulence [10, 13, 14]. At small evolution times when flow is still not-turbulent quasi-shocks and their respective jets are very visible. With time jets have a tendency to mutual overlapping but significant angular fluctuations retain in the energy distribution at the steady state.

3. The jet structures reflect also in the behavior of third-order velocity structure function $S_3^{(L)}(\mathbf{R}) = \langle (\delta v_\parallel)^3 \rangle$. Like for the isotropic direct cascade with constant enstrophy flux [20–23] fitting shows that this correlation function behaves linearly on both η and R^3, $S_3^{(L)}(\mathbf{R}) = C_3 \eta R^3$, but demonstrates a significant dependence for coefficient C_3 on angles θ, in correspondence with those observed for $\epsilon(\mathbf{k})$. Average of C_3 over angles yields for mean value $\bar{C}_3$ being far from the theoretical prediction for the isotropic turbulence (see, e.g., review [24] and references therein).

2. Mathematical model and numerical scheme. We consider the two-dimensional Navier–Stokes equation for an incompressible flow $\mathbf{u}(\mathbf{x}, t) = (u_x(x, y, t), u_y(x, y, t))$ in the vorticity formulation, $\Omega = \nabla \times \mathbf{u}$,

$$\frac{\partial \Omega}{\partial t} + (\mathbf{u}\nabla)\Omega = F + G \qquad \text{with} \quad \operatorname{div} \mathbf{u} = 0 \tag{2}$$

supplemented by the periodic boundary conditions in x and y directions in the square box with size $L = 1$. Here, F is a function responsible for both injection of the energy and its dissipation on large scales and G for enstrophy dissipation at large k.

To study the direct cascade we model F so that to eliminate influence of the energy condensation due to inverse cascade by introducing a strong dissipation at $k < k_p$, where k_p is the characteristic injection wave number. In our numerics we used function F in the form $F = \hat{\Gamma}\Omega$, where the Fourier transform of operator $\hat{\Gamma}$

$$\Gamma_k = A \frac{(k^2 - b^2)(k^2 - a^2)}{k^2} \quad \text{at} \quad 0 \leq k \leq b, \tag{3}$$

$$\Gamma_k = 0 \quad \text{at} \quad k > b. \tag{4}$$

Parameters a and b were chosen by such a way to get a rapid transition to the stationary energy dissipation at small k.

Dissipation function $G = \hat{\gamma}\Omega$ was taken in the viscous-type form:

$$\gamma_k = 0 \quad \text{at} \quad k \leq k_c, \tag{5}$$

$$\gamma_k = -\nu (k - k_c)^2 \quad \text{at} \quad k > k_c, \tag{6}$$

where viscous cut-off k_c was taken as $0.6 k_{\max}$ with $k_{\max} = 4096$ being the maximal value of k. Coefficient 0.6 in front of $k_{\max}$ provides to prevent aliasing.

Appropriate changes of boundaries $k = b$ and $k = k_c$ for zeroth values of both Γ_k and γ_k allowed us to get a maximally possible inertial interval for a given spatial resolution. Note that, in the interval $b < k < k_c$,

Eq. (2) transforms into the Euler equation. As it was shown analytically and confirmed by numerical experiments [10, 13–15] for freely decay turbulence there exists a tendency for breaking of the di-vorticity lines. This is consequence of the representation analogous to that for the 3D Euler equation, i.e. the vortex line representation [25, 26], and thereby the compressible character of the di-vorticity lines. Just this compressibility is a reason for appearance of sharp vorticity gradients in the form of quasi-shocks and respectively jets in the k-space.

Eq. (2) was solved numerically using pseudo-spectral Fourier method, while integration on time was performed with the help of hybrid Runge–Kutta/Crank–Nicholson third-order scheme. Derivatives was calculated in the spectral space, whereas the nonlinear terms were determined on a computational grid in the physical space. Convective term was approximated explicitly, and for linear terms (F and G) we used implicit scheme. The transformations from the physical to the spectral space and back were performed through the Fast Fourier Transform (FFT). Spatial resolution was 8192×8192 points. Simulations were performed (with the use of the NVIDIA CUDA technology) at the Computer Center of the Novosibirsk State University.

Initial conditions were chosen familiar to those used in our previous paper [14] as random sets of vortices with zero mean vorticity. The initial spectrum was concentrated in the region comparable with the injection scale k_c. We verified that variations in the initial conditions qualitatively did not change behavior of the system and its statistical characteristics.

3. Numerical results. First, we determined the parameters for pumping rate Γ when turbulence reached its stationary state. These are $A = 0.004$, $a = 3$, $b = 6$, and $\nu = 1.5$. Choice of the first three parameters provided sufficiently rapid transition to the stationary state for $k \leq 3$ and combination with the fourth one to approaching stationary asymptotics for the mean (average over angles) enstrophy flux.

Fig. 1 for the given parameters A, a, b, and ν shows temporal behavior of the total energy and the enstrophy. As seen total energy E tends to the constant value (stationary state) at earlier time than the total enstrophy does. In our numerical experiments we found also how the energy spectrum and both the vorticity and di-vorticity spatial distributions evolve with time.

Fig. 2 shows the angularly averaged spectrum of turbulence $E(k)$ at different instants of time. At times $t = 220$ one can see the steady (compare with Fig. 1) spectrum with the Kraichnan behavior $E(k) \sim k^{-3}$ which is seen almost on three decades. At the steady state ($t \gtrsim 200$) by calculating the enstrophy flux η as

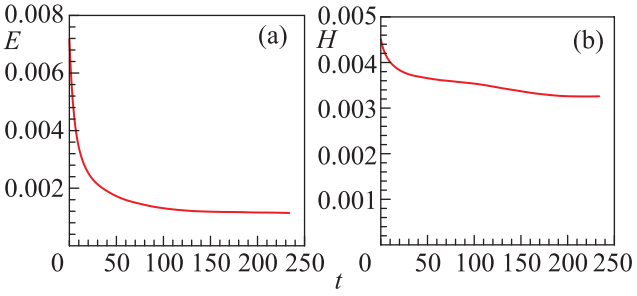

Fig. 1. (Color online) Time evolution of total energy E and total enstrophy H

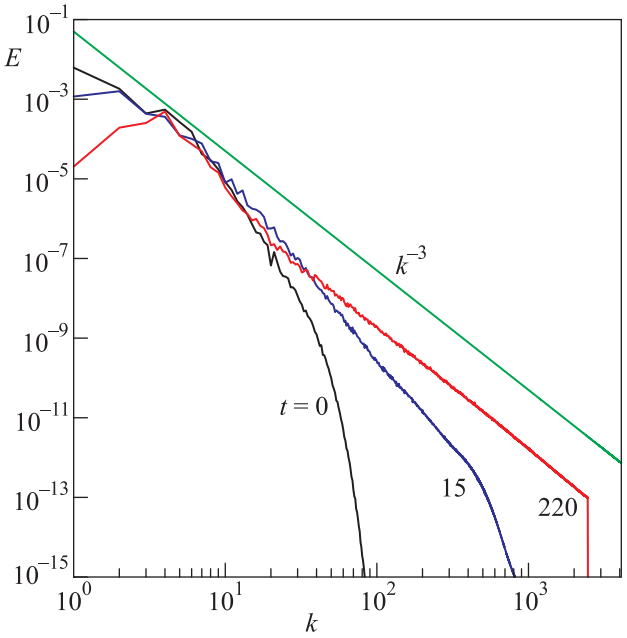

Fig. 2. (Color online) Energy spectrum $E(k)$ at different instants of time

the integral $\int \gamma(k)|\Omega(\mathbf{k})|^2 d\mathbf{k}$ we verified that the steady energy spectrum $E(k)$ with a high accuracy coincides with the Kraichnan spectrum $E(k) = C_{\mathrm{K}}\eta^{2/3}k^{-3}$, where $C_{\mathrm{K}} \simeq 1.3$ the Kraichnan constant, in correspondence with the previous simulations [16–19].

As was shown [10, 13, 14], for the decay turbulence such a spectrum is formed owing to the sharp vorticity gradients appearing due to breaking of di-vorticity lines. Results presented in Figs. 3–5 also show a significant role of this process on the formation of the Kraichnan spectrum. In Fig. 3 one can see the spatial distributions of Ω at $t = 100$, before reaching the steady state, and at $t = 220$, after its reaching. These are typical distributions for Ω, but they are less informative than the corresponding distributions of di-vorticity $|\mathbf{B}(\mathbf{r}, t)|$ which are presented in Fig. 4 (for the same time instants as in Fig. 3).

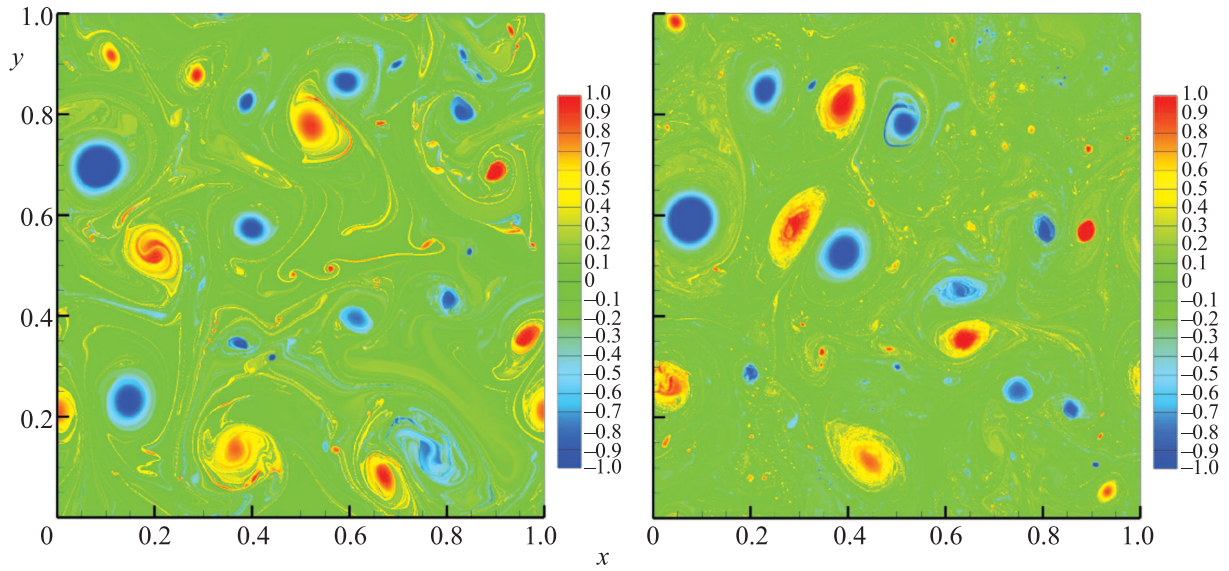

Fig. 3. (Color online) Vorticity distributions at $t = 100, 220$

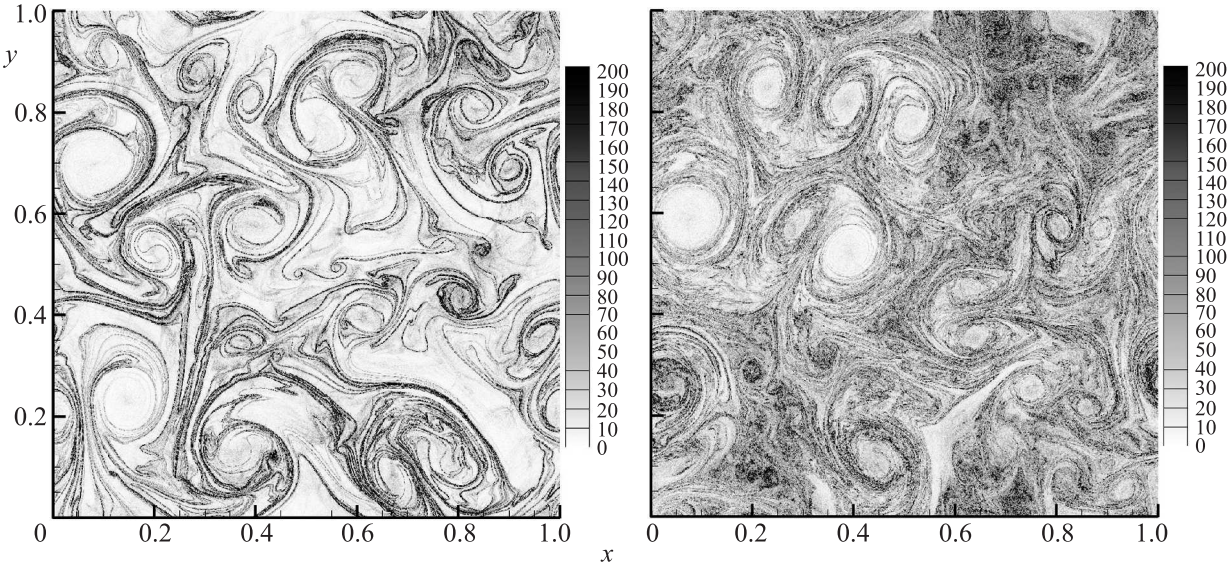

Fig. 4. Distribution of $|\mathbf{B}|$ at $t = 100, 220$

As is seen from these figures the di-vorticity value concentrates along lines which form a whole network, between these lines $|\mathbf{B}|$ is much less. This difference is most clearly seen in the dependence of $|\mathbf{B}|$ along projection $y = 0.5$ (see Fig. 5) where maxima of the di-vorticity exceed its minimal values for 1–2 orders of magnitude.

These maxima define positions of the vorticity quasi-shocks which in the k-space, due to jets, are responsible for anisotropy in 2D energy distribution $\epsilon(k_x, k_y)$. Fig. 6 shows 2D compensated spectrum $k^4\epsilon(k_x, k_y)$ for the steady state where one can see a set of jets with both strong and weak mutual overlapping.

Along each such jets $\epsilon \sim k^{-4}$ which after angular average leads with a high accuracy to the Kraichnan spectrum.

However, anisotropy, due to quasi-shocks, plays a more significant role for the higher moments of the velocity field than for the spectrum. Fig. 7 shows the dependencies of the third-order velocity structure function $S_3^{(L)}(\mathbf{R}) = \langle(\delta v_\parallel)^3\rangle$, depending on R for various values of angles, where $\mathbf{R} = \mathbf{r} - \mathbf{r}'$ and $\delta v_\parallel$ – the projection of the velocity difference onto the vector $\mathbf{R}$. At each angle $S_3^{(L)}(\mathbf{R})$ is close to the cubic parabola, i.e. $\propto R^3$, with a linear dependence relative η. However, the average of the third-order velocity structure function over an-

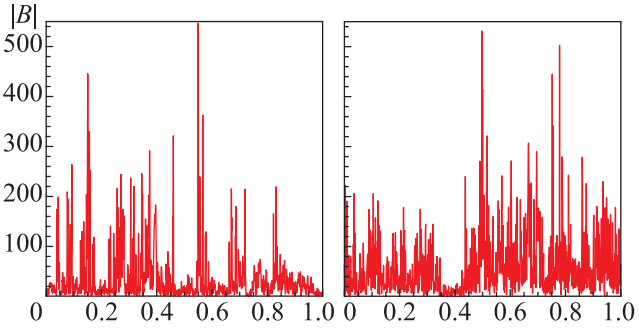

Fig. 5. (Color online) Distribution of $|\mathbf{B}|$ along line $y = 0.5$ at $t = 100, 220$

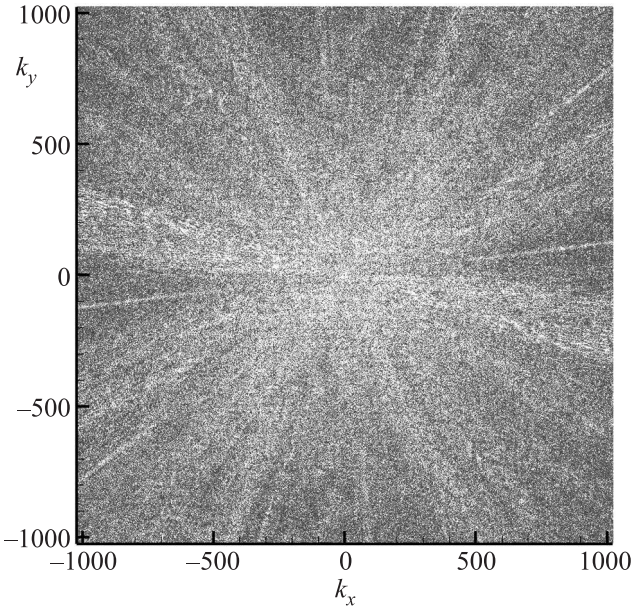

Fig. 6. 2D compensated spectrum $k^4\epsilon(k_x, k_y)$ at $t = 220$

gles only gives a significant difference with the constant $C_{3,\mathrm{isotr}} = 1/8$ for the isotropic turbulence. However, the angular averaging constant C_3 undergoes temporal fluctuations: its maximal value sometimes reaches 5 (for this "steady" state!). Average over time within window $210 \geq t \leq 465$ with characteristic period $\simeq 17$ gives better correspondence: $\bar{C}_3 \simeq 2.4 C_{3,\mathrm{isotr}}$.

4. Conclusion. The main resume of this work is the fact that for the 2D turbulence, in the presence of pumping and damping, quasi-shocks, originated because of compressibility of di-vorticity lines, play very essential role in the direct cascade. Quasi-shocks are key factors which define 2D turbulence anisotropy, in particular, anisotropy of both spectrum and structure functions. Surprisingly that averaging over angles of 2D energy distribution $\epsilon(k_x, k_y)$ gives with a high accuracy the Kraichnan spectrum. This result coincides with results of the previous numerical experiments [16–19]. Note,

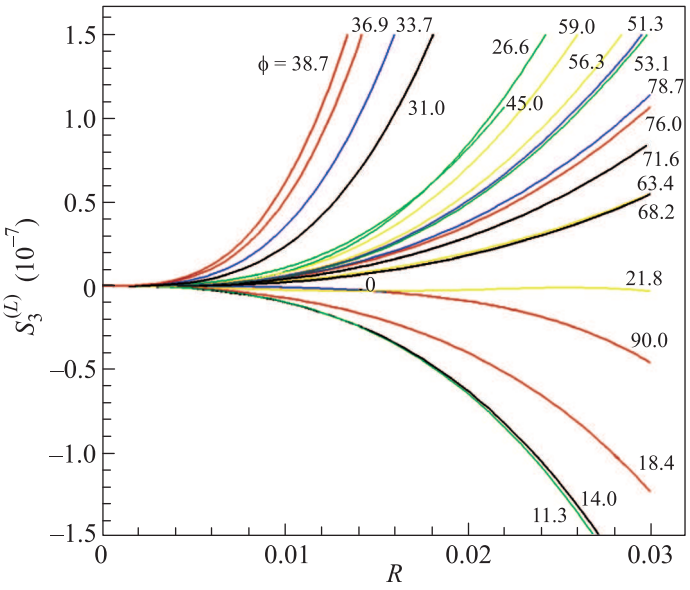

Fig. 7. (Color online) Dependence of $S_3^{(L)}$ as function of R at different angles

the same averaging for the third-order velocity structure function yields a value for constant $\bar{C}_3$ different from a pure isotopic case (see, e.g., review [24] and references therein), in spite of the correct dependence of $S_3^{(L)}$ on both enstrophy flux η and separation R. This is an open question which we are going to study in our future work.

The authors thank A.N. Kudryavtsev and G.E. Falkovich for useful discussions. This work was supported by the RSF (Grant # 14-22-00174).

1. R. Kraichnan, Phys. Fluids **11**, 1417 (1967).
2. D. K. Lilly, J. Fluid Mech. **45**, 395 (1971).
3. J. C. McWilliams, J. Fluid Mech. **146**, 21 (1984).
4. S. Kida, J. Phys. Soc. J. **54**, 2840 (1985).
5. M. E. Brachet, M. Meneguzzi, and P. L. Sulem, Phys. Rev. Lett. **57**, 683 (1986).
6. M. E. Brachet, M. Meneguzzi, and P. L. Sulem, J. Fluid Mech. **194**, 333 (1988).
7. R. Benzi, S. Patarnello, and P. Santangelo, Europhys. Lett. **3**, 811 (1986).
8. B. Legras, B. Santangelo, and R. Benzi, Europhys. Lett. **5**, 37 (1988); B. Santangelo, R. Benzi, and B. Legras, Phys. Fluids A **1**, 1027 (1989).
9. K. Okhitani, Phys. Fluids A **3**, 1598 (1991).
10. E. A. Kuznetsov, V. Naulin, A. H. Nielsen, and J. J. Rasmussen, Phys. Fluids **19**, 105110 (2007).
11. P. G. Saffman, Stud. Appl. Math. **50**, 49 (1971).
12. W. Wolibner, Math. Z. **37**, 698 (1933); V. I. Yudovich, **3**, 1407 (1963); T. Kato, Arch. Rat. Mech. Anal. **25**, 189 (1967).

13. E. A. Kuznetsov, V. Naulin, A. H. Nielsen, and J. J. Rasmussen, Theor. Comput. Fluid Dyn. **24**, 253 (2010).
14. A. N. Kudryavtsev, E. A. Kuznetsov, and E. V. Sereshchenko, Pis'ma ZhETF **96**, 783 (2012) [JETP Lett. **96**, 699 (2013)].
15. E. A. Kuznetsov, Pis'ma v ZhETF **80**, 92 (2004) [JETP Lett. **80**, 83 (2004)].
16. T. Gotoh, Phys. Rev. E **57**, 298491 (1998).
17. N. Schorghofer, Phys. Rev. E **61**, 657277 (2000).
18. E. Lindborg and K. Alvelius, Phys. Fluids **12**, 945 (2000).
19. E. Lindborg and A. Vallgren, Phys. Fluids **22**, 091704 (2010).
20. U. Frisch, *Turbulence: The Legacy of AN Kolmogorov*, Cambridge Univ. Press, Cambridge, UK (1995).
21. D. Bernard, Phys. Rev. E **60**, 618487 (1999).
22. E. Lindborg, J. Fluid Mech. **388**, 259 (1999).
23. V. Yakhot, Phys. Rev. E **60**, 5544 (1999).
24. G. Boffetta and R. E. Ecke, Annu. Rev. Fluid Mech. **44**, 427 (2012).
25. E. A. Kuznetsov and V. P. Ruban, Pis'ma v ZhETF **67**, 1015 (1998) [JETP Lett. **67**, 1076 (1998)]; Phys. Rev. E **61**, 831 (2000).
26. E. A. Kuznetsov, Pis'ma v ZhETF **76**, 406 (2002) [JETP Lett. **76**, 346 (2002)].